Identifying interfacial failure mode in aerospace adhesive bonds by broadband dielectric spectroscopy

Nijemeisland, Marlies; Meteleva-Fischer, Yulia V.; Garcia, Santiago J.

DOI
10.1016/j.ijadhadh.2022.103246

Publication date
2022

Document Version
Final published version

Published in
International Journal of Adhesion and Adhesives

International Journal of Adhesion & Adhesives 118 (2022) 103246

Contents lists available at ScienceDirect

International Journal of Adhesion and Adhesives

journal homepage: www.elsevier.com/locate/ijadhadh

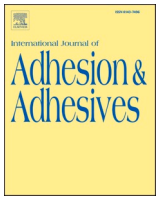

Identifying interfacial failure mode in aerospace adhesive bonds by broadband dielectric spectroscopy

Marlies Nijemeisland [a], Yulia V. Meteleva-Fischer [b], Santiago J. Garcia [a,*]

[a] Novel Aerospace Materials Group, Faculty of Aerospace Engineering, Delft University of Technology, Kluyverweg 1, 2629 HS, Delft, the Netherlands
[b] GKN Fokker Aerostructures B.V., Industrieweg 4, 3351 LB, Papendrecht, the Netherlands

ARTICLE INFO

Keywords:
Dielectric spectroscopy
Durability
Non-destructive testing
Interfacial failure
Adhesive bonding

ABSTRACT

The most widely accepted test for bond durability analysis in aerospace metal-bonded structures is the bondline corrosion test introduced in the late 90s. Little progress has been made however on non-destructive testing methods that allow determining the bond quality after years of use. Here, a non-destructive method based on dielectric spectroscopy is introduced to evaluate the state of a metal-adhesive-metal bond exposed to salt fog spray up to 180 days. Several samples were evaluated with broadband dielectric spectroscopy (BDS), floating roller peel (FRP) tests and bondline corrosion (BLC) after exposure to salt fog spray test for different times. Relaxation processes and conductivity phenomena extracted from the BDS data (e.g. apparent conductivity relaxation time (τ_{max}) using electric modulus) are found to correlate well with the bond strength measured in peel test and BLC progression. The BDS-based protocol was able to identify the local interfacial degradation stages in a non-destructive mode and with high resolution. The protocol has the potential to be further developed into a test method for durability on coupon level.

1. Introduction

Adhesive bonding is used since the 50s to join metallic materials and since more recently composite materials for aerospace applications [1, 2]. Despite the proven value of bonding technologies in complex structures and joints, numerous factors have been found to alter the bond properties of adhesive joints, such as the anodizing process, curing time, primer layer thickness, type of adhesive film, or exposure to marine environment [3–5]. Any of these factors can affect the bond quality and possibly lead to a weak bond between the two surfaces with the consequent loss in structural integrity. A better understanding of the behavior of adhesive bonds and their ageing process is necessary for the design of new type of bonds with improved durability.

One of the tests used to study durability with defined qualification requirements is the bondline corrosion test introduced by Airbus Industries in the late 90s [6]. The test is dedicated to a special form of corrosion developing over time in adhesively bonded structures made of clad aluminium alloy, sometimes named after the proprietary name Alclad. In this destructive test, floating roller peel specimens are manufactured, exposed to neutral salt spray (NSS) per ASTM B117 for a specified period of time (e.g. 45, 90, 180 or 300 days), peeled open, and the amount of corrosion as well as percentage of adhesive/cohesive fracture mode are calculated [7]. The obtained data is compared to the limits experimentally established from airplane inspections over 30 years of service. Pethrick et al. provided insight in the number of processes that can decrease the bond strength after NSS exposure such as swelling and plasticisation of the adhesive, and ingress of water along the polymer-polymer and polymer-metal/oxide interfaces [8]. The build-up of moisture and salt at the interface in turn promotes corrosion and bond breakage thereby deteriorating the adhesive bond structure and strength. The existing testing protocols, such as the bondline corrosion test, which are useful to ballpark the durability of new bond structures, tend to be time consuming and costly besides being destructive. Moreover, such destructive testing does not allow for in-field evaluation of bonded structures to estimate the quality of the bond after years in use. Therefore, the search for evaluation methods that are able to provide discriminative local information about the bond strength and degradation stage and type, that are faster and allow testing of bonded parts in use (i.e. in a non-destructive fashion) are still subject of research. NDTs such as ultrasonic testing or thermography have been proposed. Nevertheless, the scale at which these NDTs detect damages/heterogeneities is significantly higher than the scale at which

* Corresponding author.
E-mail address: s.j.garciaespallargas@tudelft.nl (S.J. Garcia).

https://doi.org/10.1016/j.ijadhadh.2022.103246
Received 28 February 2022; Accepted 15 July 2022
Available online 10 August 2022

interfacial damages occur; therefore these techniques have not been able to show reproducible and reliable information about the bond quality and the detection of weak bonds [9–14]. Laser shock peening technique was successfully applied for the detection of weak bonds in laminate composites [14]. Nevertheless, its use for aluminium bonded structures is limited as laser peening interferes with the known process of local metal strength modification resulting in the enhancement of fatigue properties [15]. An alternative to these could be the use of techniques able to detect variations in the material dynamics (temperature and frequency dependent) at the molecular scale such as broadband dielectric spectroscopy (BDS).

BDS studies the interaction of an external electric field with electronic dipoles present in the target sample (e.g. dipolar molecules) as a function of frequency, often expressed as permittivity. A variety of dielectric responses in materials have been reported ranging from dielectric relaxation, ionic relaxations, dipole relaxations in the low frequency range (10^{-2}-10^{9} Hz) up to atomic ($\sim 10^{12}$ Hz) and electronic polarizations ($\sim 10^{15}$ Hz) in the high frequency range [16]. The study and understanding of such relaxation modes and their relation to, for instance polymer relaxation dynamics, led to the use of BDS to evaluate the presence and impact of heterogeneities in materials. Some examples include polymer morphology variations in polymer blends as shown by Rathi et al. [17], the presence of particles with different dielectric response and phase orientation as demonstrated by Maity et al. and Li et al. [18,19] or the presence of molecular and macroscopic damage in elastomers and their healing as shown by Hernández et al. [20]. Moreover, BDS was recently used by Wübbenhorst et al. to demonstrate that the dynamics of monomers or/and polymers in pores strongly depend on the level of restriction (i.e. mechanical interlocking and bond type with the pore walls) [21].

In this study, BDS results are correlated with bond strength in aerospace adhesive joints obtained with destructive testing. In a quasi-quantitative way, the effect of NSS exposure on bondline corrosion and bond strength were studied in a non-destructive manner with BDS. Although progress has been made in the use of BDS to study the performance of adhesive bonds such as described by Banerjee, Elenchezhian et al. [22,23], the proposed methodology is not suitable for adhesive bonds with a significant conductive component. Fillers, impurities or moisture can obscure interfacial relaxations by introducing conductivity phenomena when represented as dielectric permittivity, as shown by Tsangaris et al. [24].

In this work, the electric modulus formalism, first introduced by McCrum et al. [25] and defined as the inverse of the complex relative permittivity, is exploited and found to be capable of revealing interfacial relaxation processes related to adhesive bond performance after NSS exposure. To this aim, a set of adhesively bonded specimens were prepared with both the Cr(VI)-free phosphoric-sulphuric acid anodization process (PSA) and the thin film sulphuric acid anodization process (TFSAA) to yield specimens with different bonding capability as shown by Abrahami et al. [3,4].

The bonded specimens were exposed to NSS and tested with BDS, standard destructive floating roller peel test (FRP) and bondline corrosion (BLC) after different exposure times to NSS. Absorbed water and salts in the polymer adhesive resulted in additional relaxation processes and conductivity phenomena compared to as produced samples, which in turn depended on which anodic anodization process was used.

A clear correlation was found between BDS data and the bondline strength measured with more traditional destructive methods. Moreover, besides being non-destructive, BDS proved being more sensitive to detect local degradation differences for same exposure times (i.e. metal-adhesive interface failure or cohesive failure and corrosion). The results suggest that BDS may be a useful technique to study adhesive bonds as well as to evaluate bondline strength and degradation in in-use bonded structures.

2. Materials and methods

2.1. Adhesively bonded specimens

Two sets of clad aluminium alloy AA7075-T6 adhesively bonded specimens were manufactured at GKN Fokker Aerostructures B.V. (NL) using the same commercial thermoset, modified epoxy, structural adhesive (3 M™ Scotch-Weld™ Structural Adhesive Film AF 163-2K.06). The surfaces of the first set were pre-treated with the PSA process while the second set was prepared by using the TFSAA process. The anodizing conditions and abbreviations used along the manuscript are summarized in Table 1. SEM measurements were used to determine oxide thickness and pore size at the surface.

In order to reduce the amount of interfaces and to facilitate data interpretation, no adhesive primer was used in this work as would normally be applied during manufacturing of adhesively bonded aluminium structures. The adhesive film *AF163-2K.06* was applied between a thin (0.8 mm) and a thick (1.6 mm) equally anodized plate in a conditioned environment (18–24 °C and RH between 25 and 60%) and cured at 125 ± 5 °C at 600 kPa with a heating rate of 1.2–2 °C/min and a total curing time of 75 min using a laboratory press equipment. Once the panels were manufactured they were cut for the different tests, whereby the side edges of 5–10 mm were discarded. The cutting scheme with the assignment of the samples for BDS, floating roller peel test (FRP) and bondline corrosion (BLC) testing are given in Fig. 1. The samples are coded with the anodizing process (PSA or TFSAA), followed by the position in the panel from where they were cut off and by the exposure time in days. Samples for BLC and FRP tests were cut in 250 ± 0.5 × 25 ± 0.5 mm. Samples for BDS were cut again in pieces of 25 ± 0.5 × 25 ± 0.5 mm.

The cut out samples as shown in Fig. 1 were either directly evaluated with destructive (dry-wet floating roller peel test) and non-destructive testing (BDS) or exposed to NSS for 45, 90 and 180 days according to ASTM B117 and then tested with destructive (dry floating roller peel test with bondline corrosion analysis) and non-destructive (BDS) techniques. All samples were dried similarly at RT in a desiccator for one week prior to testing.

2.2. Scanning electron microscopy

Oxide thickness and pore size were measured from cross-section and top view using a JEOL JSM 7500F Scanning Electron Microscope. Samples were coated with a 15 nm gold layer before SEM examination. Image capturing was performed at an accelerating voltage of 5.0 keV, a current of 10 μA and a working distance of 3.0–4.5 mm. The JEOL image software was used to measure pore distances and layer thickness.

2.3. Dry-wet floating roller peel test (FRP) and BLC

In industry, the bond quality is determined by the floating roller peel strength and the fracture mode of the adhesive bond; where the first has to be above the requirements for the structural adhesive system, and the

Table 1
Summary of the pre-treatment conditions.

Process abbreviation	Pre-treatment	Conditions
PSA	Fokker phosphoric acid anodizing [26]	10–40 g/L sulphuric acid and 4–16 g/L phosphoric acid 42–48 °C 15–25 V 30 min
TFSAA	A variation of thin film sulphuric acid anodizing	10 g/L sulphuric acid 20 °C 27 V 30 min

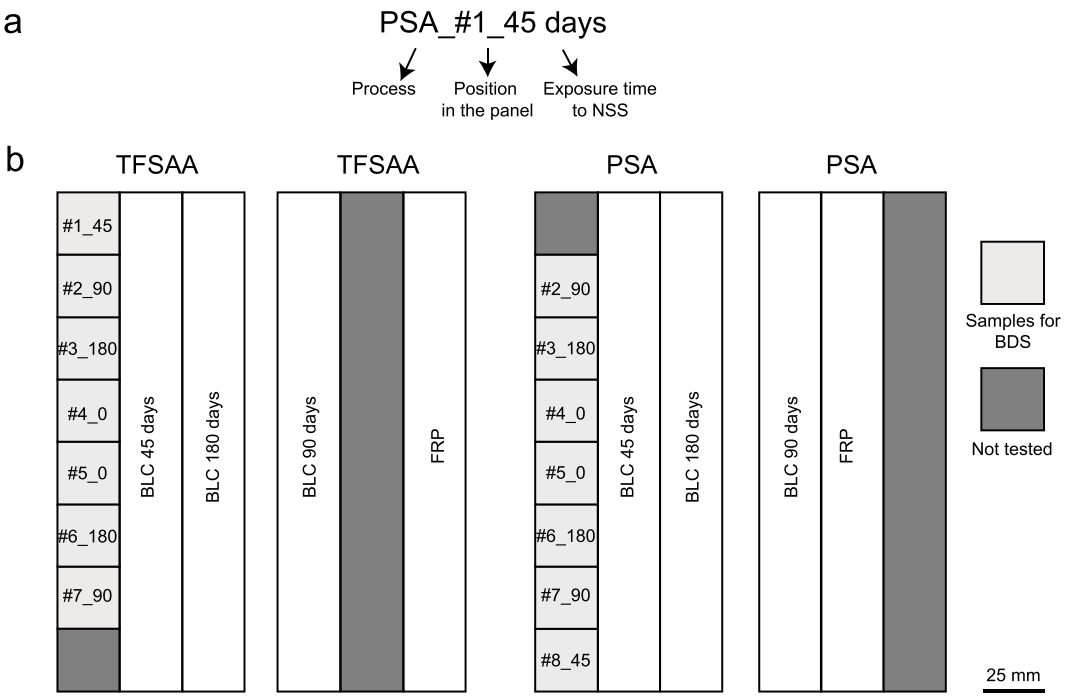

Fig. 1. Sample code used in this work (a) and cutting scheme from manufactured adhesive bonds to be tested in BDS, BLC and FRP (b). The position of the cut out samples was selected to ensure representative results and to not account for edge effects (note: side edges of 5–10 mm were discarded).

second has to be predominantly cohesive [27].

The floating roller peel test was executed per ASTM D3167 using Instron 5500R tensile machine in dry and wet mode for the non-exposed samples and in dry mode for the samples pre-exposed to the neutral salt fog spray test (NSS) per ASTM B117. First, the specimen is peeled up to at least 80 mm length as is (dry mode), then a droplet of water is added into the crack tip while peel continues with the same speed of 100–120 mm/min. Wet peel represents the performance of a specimen free of weak bonds that will degrade as first when exposed to the salt spray. For the bond strength calculation a minimum peeled length of 180 mm was used for the dry tested samples (i.e. those exposed to NSS). A minimum of 80 mm was used for the dry/wet specimens. The peel plots were recorded for each specimen and their fracture mode was optically determined. The bondline corrosion (BLC) percentage and fracture mode (% of cohesive failure) were calculated optically from the peeled opened specimens using the guidelines of AITM5-0009. It should be noted that the dry-wet floating roller peel tests is considered even more discriminating than the wedge test per DIN 65448, introduced by Boeing for evaluation of durability of adhesive joints [28–31].

2.4. Broadband dielectric spectroscopy (BDS)

Dielectric spectroscopy measurements were performed in a broadband dielectric spectrometer system based on an Alpha-n analyser and Quatro temperature controller (Novocontrol Technologies GmbH). Upper and bottom surfaces of the specimens tested in BDS were polished to ensure good ohmic contact with the BDS electrodes. The four laterals of the samples were also polished to remove corrosion products, salts or imperfections from the cutting process in order to avoid any possible bridging between electrodes. After polishing, the samples were mounted in a dielectric cell between two parallel gold-plated electrodes with a diameter of 20 mm to ensure high quality electrode contact and thereby reducing electrode polarization due to poor contact. In this way, the bonded structure acts as a capacitor where the adhesive is the dielectric and the aluminium plates are the electrodes. No signs of electrode polarization were detected as a confirmation of a good contact between the samples and the BDS electrodes.

In order to analyze the effect of entrapped humidity on the BDS signals, the samples taken after the shortest exposure time, 45 days, were tested short after NSS exposure and after one week drying in a desiccator containing dried silica gel beads.

The complex permittivity $\varepsilon^*(\omega) = \varepsilon'(\omega) - i\varepsilon''(\omega)$ of each sample was measured by performing consecutive isothermal frequency sweeps with an oscillating voltage of 1 V_{rms} over a frequency window of $10^{-1} <$ f (Hz) $< 10^7$ (where $f = \frac{\omega}{2\pi}$ is the frequency of the applied electric field, where ω is the angular frequency), at 47 different frequencies in the temperature range from −100 to 0 °C in steps of 10 °C.

After BDS and FRP testing, all the samples were mechanically opened. Photographs were taken with a digital camera and analyzed with ImageJ to estimate the percentages of interfacial and cohesive fracture modes as well as percentage of the bondline corrosion on both the thin and the thick plates of the bond following the AITM5-0009 [6].

3. Results and discussion

3.1. Anodized layer morphology

Fig. 2 shows representative scanning electron microscopy (SEM) images of the anodized samples obtained using PSA and TFSAA processes in order to visualize differences in oxide thickness, pore size and oxide surface morphology. Image analysis shows that the PSA process produces anodized oxide layers with a columnar structure with pore-dimension of 15–20 nm and a layer thickness of around 3 μm. Moreover, the PSA oxide shows the presence of "bird-nest" structures on the surface (Fig. 2b). Abrahami et al. reported this to be due to the dissolution of the anodic oxide during the PSA process and considered this to favour high adhesive bond quality [4]. The TFSAA process on the other hand leads to a denser honeycomb structure with finer pores (6–10 nm) and a layer thickness of approximately 2.5 μm. The influence of anodizing chemistry on the oxide structure was first acknowledged in the PABST program [29,32].

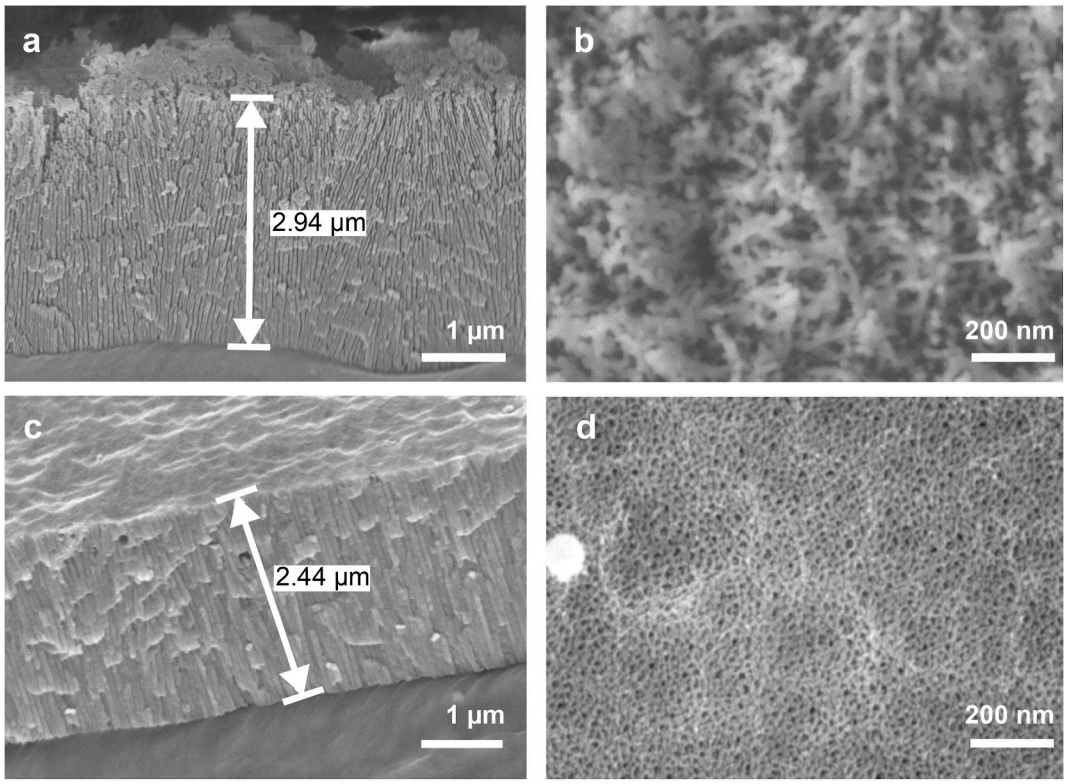

Fig. 2. SEM images of the surface morphology of the oxides produced with PSA (a for side view and b for top view) and TFSAA (c for side view and d for top view).

3.2. Non-destructive testing: relaxation dynamics by BDS

3.2.1. Behavior of the adhesive bonds before exposure to NSS

Before exposing the samples to neutral salt spray, two sets of samples produced with the two anodizing processes were studied with BDS. This allowed evaluating the effect of the anodizing process (PSA or TFSAA) on the secondary relaxations and the glass transition temperature of the adhesive bonds.

Fig. 3a shows representative BDS results of the two systems shown as imaginary dielectric permittivity vs. temperature at 100 Hz. Fig. A1 shows the real and imaginary dielectric permittivity with frequency at various temperatures. As for most amorphous polymers, two relaxation regions related to the thermoset adhesive, can be observed in the temperature domain which was consistent with previous results [33]. At low temperatures, a broad peak can be observed in the dielectric loss curve. This relaxation (β-relaxation) in amorphous polymers is, in general agreement with previous work, assigned to localized rotational fluctuations of the dipole vector [34]. The α-relaxation, attributed to a dynamic glass transition, is observed at higher temperatures and attributed to coordinated large scale motions of the polymer chains [35]. No clear differences are observed between process TFSAA and PSA on the molecular relaxations before exposure to NSS.

In order to better show the trends for the β-relaxation, the dielectric loss vs, frequency at different temperatures was used (Fig. 3b, shows the example for TFSAA system). In this figure it can be seen how f_{max}, the frequency at the peak maximum of ϵ'' for the β -relaxation, increases with increasing temperature. This indicates faster molecular motions and shorter relaxation times. Apparent relaxation times for the β-relaxation can be determined as $\tau_{max} = 1/(2{\cdot}\pi{\cdot}f_{max})$, where f_{max} denotes the frequency of the maximum of the β -peak. Log τ_{max}, when plotted against 1/T (see Fig. 3c), shows strong Arrhenius behavior according to the following equation (Eq. (1)),

$$\tau_{max}(T) = \tau_0 \exp\left(\frac{E_a}{RT}\right) \quad \text{(Eq. 1)}$$

with Ea, the activation energy for this β-relaxation. Both anodizing treatments lead to comparable activation energies (~31 kJ/mol for TFSAA_#0_0days and ~ 26 kJ/mol for PSA_#0_0days). This suggests that the surface chemistry and oxide morphology due to the anodization process do not affect the secondary relaxations in the glassy state of the polymers before NSS.

3.2.2. Behavior of the adhesive bonds after exposure to NSS

The adhesive bonds using the two anodizing protocols were exposed to NSS in duplicate and evaluated by BDS after different exposure times (different specimens per exposure time). Fig. 4a shows, as a mode of example, the BDS results (dielectric loss vs frequency) of a TFSAA sample exposed to NSS for 45 days. In Fig. 4a significantly higher values of ϵ'' are observed at low frequencies when compared to the results obtained for the specimens not exposed to NSS (Fig. 3b). In addition, the dielectric loss increases with temperature in the whole frequency range and indicates the presence of thermally activated processes. The larger values of permittivity after NSS exposure can be attributed to the so-called electrode polarization effect, proposed by Kremer et al. [16], and suggest higher charge mobility. The significant drop of the permittivity becomes more visible at higher frequencies. This suggests a restriction to the charge diffusion phenomena, and the temperature dependency possibly due to the accumulation of moisture and salts at the adhesive bond (adhesive-anodized layer interface and adhesive self) due to the exposure to NSS. To confirm the source of the electrode polarization related to moisture, the same specimens were dried for two weeks prior to the BDS test. After drying, the conductivity relaxation peak dropped considerably (Figure B1). This indicates a strong reduction of mobile charge carriers and supports the hypothesis that the electrode polarization is caused by the combination of moisture and salt ingress.

A saturation effect is also observed at higher frequencies, while the high values in the low frequency range represent ion conduction. The constant value of ε'' at high frequencies is because interfacial polariza-

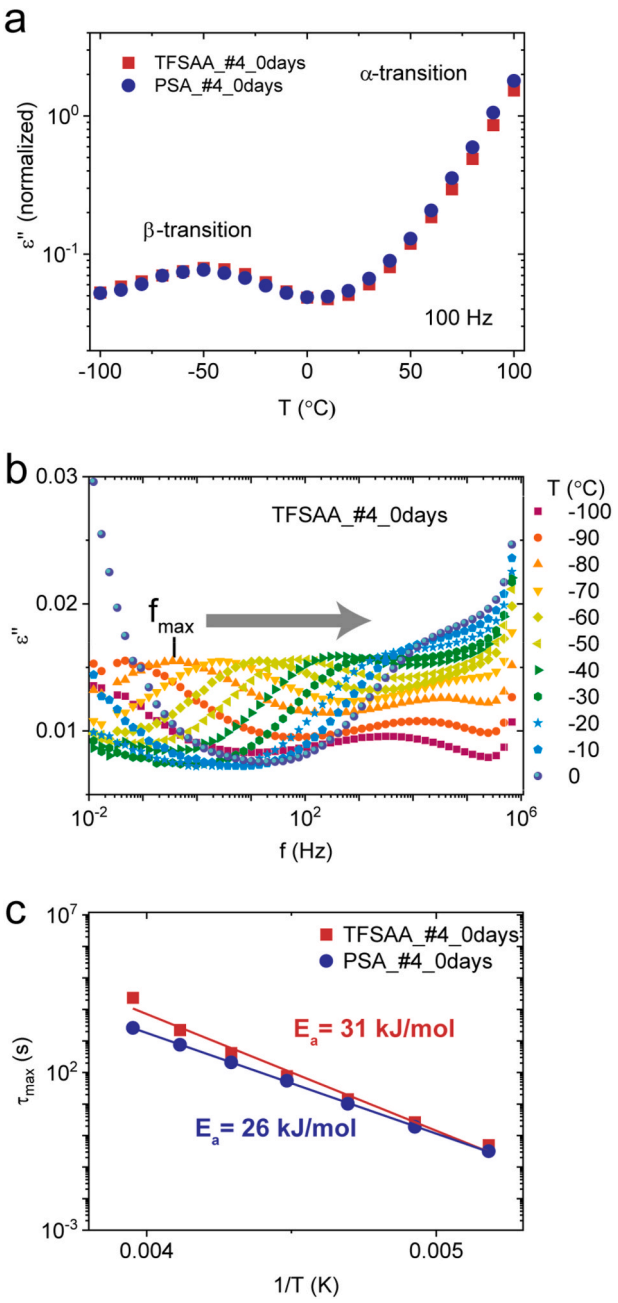

Fig. 3. Typical variation of (a) imaginary normalized dielectric permittivity (ϵ″) with temperature at 100 Hz at t = 0 days (b) imaginary dielectric permittivity (ϵ″) with frequency at various temperatures for TFSAA bonded panels at t = 0 days and (c) the apparent relaxation time as function of temperature, following strong Arrhenius behavior for the two studied bonding processes (PSA and TFSAA).

tion is ineffective at higher frequencies, as large dipoles developed at the interfaces cannot follow the electric field when the frequency is high. The above observations highlight that the electrode polarization reflected in the dielectric permittivity (as shown in Fig. 4a) is very dominant and suppresses other relevant relaxation processes. Since one of the intentions of this work was to explore the potential of BDS as a NDT method to evaluate the state of adhesive bonds right after exposure to aggressive solutions, it was decided to avoid extended drying. As a consequence, due to electrode polarization interference, dielectric permittivity cannot be used directly to interpret the BDS results. An alternative approach correcting for this interference had to be implemented as shown here below.

In order to correct for the electrode polarization and to obtain a better insight into the relaxation processes at lower frequencies, the modulus formalism was applied as described in Ref. [36]. This formalism uses the electric modulus M^*, which is defined as the inverse of the complex dielectric permittivity ε^* (Eq. (2)),

$$M^* = \frac{1}{\varepsilon^*} = \frac{(\varepsilon' - i\varepsilon'')}{|\varepsilon^*|^2} = M' + iM'' \quad \text{(Eq. 2)}$$

with M' and M'' as the real and imaginary part of the complex modulus M^*.

In practice, the use of the electric modulus allows suppressing large values of permittivity and conductivity at low frequencies due to electrode polarization. Although still under debate due to its indirect way of measuring the coupled conductivity and dielectric relaxation [37], the use of M^* is broadly applied to study: (i) polymeric electrolytes to separate bulk relaxation phenomena from the ionic relaxation and where the relaxations are speculated to occur from ionic motion, and (ii) systems with a conductive component (e.g. a polymer with conductive particles) where the relaxation processes are often obscured by conductivity phenomena as noted in Ref. [38]. In this work, the use of the electric modulus (M^*) decreased the conductivity effect (induced by the ingress of salt solution during the NSS exposure) and highlighted the relevant features occurring at higher frequencies. This allowed simplifying the interpretation of the BDS data and the study of the effect of NSS exposure on the durability of the adhesive bonds.

Fig. 4b and c shows representative plots of the imaginary part of the electric modulus (M'') at different temperatures for TFSAA _#1_45days and PSA_#8_45days respectively. The use of the electric modulus formalism leads to the clear identification of a relaxation peak in both sample series (TFSAA and PSA) which was not evident in the dielectric loss plot (Fig. 4a).

Kremer et al. proposed that the left side of the M'' relaxation peak (low frequencies) represents the range where charge carriers are mobile from one site to the neighboring site, while the region to the right is the range where bound ionic dipoles are spatially confined to their potential well [16]. The frequency range where the peak occurs is indicative for the transition from long-range to short-range mobility of charge carriers. The shift of the relaxation peak towards higher frequencies with the temperature indicates that the movement of charge carriers is a thermally activated process that becomes faster with temperature, as noted in Ref. [39]. It can be seen that the M'' spectra are asymmetric and skewed towards the higher frequency side of the maxima. This broad and asymmetric nature indicates a wide distribution of conductivity relaxation processes of charge carriers and thus heterogeneity in the measured area (i.e. the adhesive bond between the electrodes). When comparing the TFSAA and PSA plots at 45 days of exposure (4b and 4c), it can be seen that the relaxation peak of PSA appears at lower frequencies than the peak of TFSAA. This suggests slower dynamics and smaller temperature influence, and therefore the presence of a more stable (i.e. better) adhesive bond. This observation correlates with previous reports suggesting that bigger pore sizes (15–20 nm) and/or the presence of oxide "bird-nest" structures as obtained in the PSA anodization lead to higher adhesive bond quality than smaller pore sizes (6–10 nm) and/or no "bird-nest" structure.

In addition to the primary relaxation peak, an additional relaxation peak was observed for both TFSAA and PSA specimens in the frequency range 10^5–10^7 (Table C1). This relaxation appeared more evident and even dominant in some samples, even for comparable exposure times (e.g. TFSAA_90 days samples #1 and #2 in Table C1), and suggests additional relaxation and conductivity phenomena at high frequencies which may be associated with the diffusion of water into the adhesive.

In order to be able to compare all samples in a quantitative manner and to study their evolution with the exposure time to NSS, the conductivity relaxation times of the primary relaxation peak were calculated using the following relation (Eq. (3)) at each studied temperature,

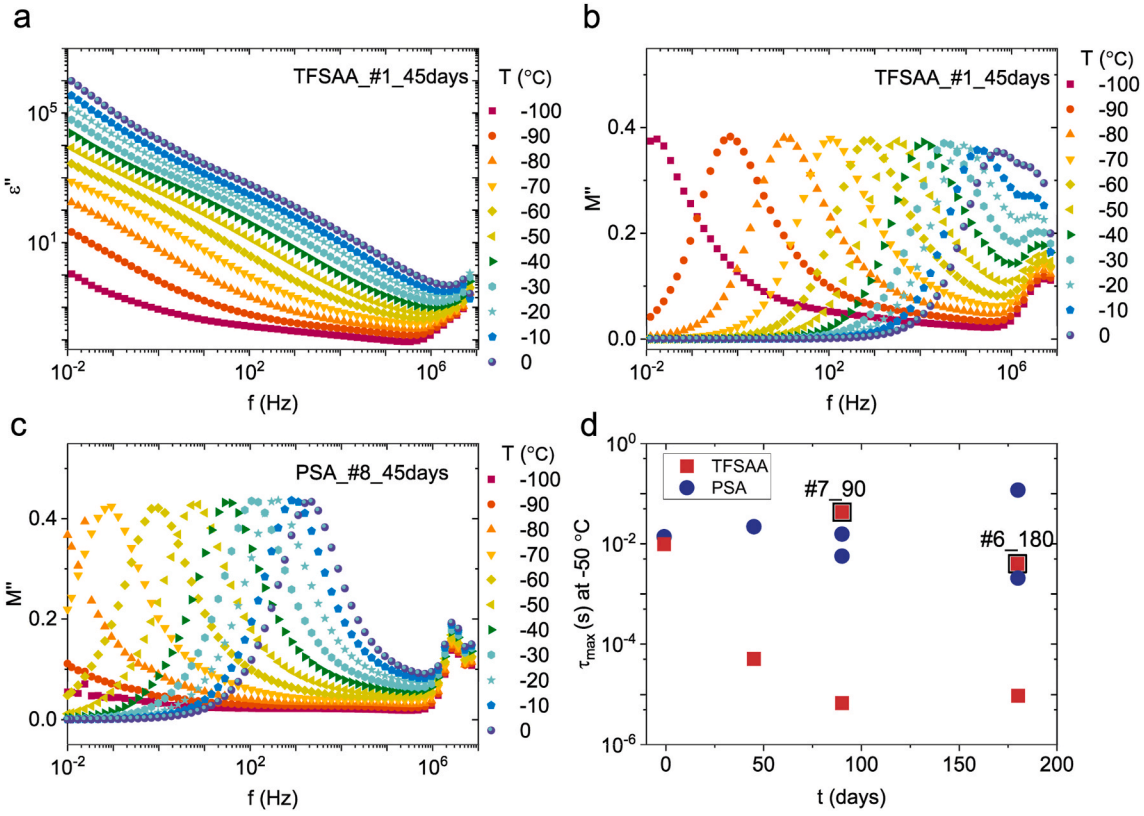

Fig. 4. (a) Dielectric loss permittivity of sample TFSAA_#1_45days shows dominant electrode polarization. By using the modulus formalism, large values of permittivity and conductivity can be suppressed as shown in (b) TFSAA_#1_45 days and (c) PSA_#8_45days. Apparent conductivity relaxation times (τ_{max} at −50 °C) for panels TFSAA and PSA as function of exposure time (d). Samples TFSAA_#7_90 and TFSAA_#6_180 highlighted with black squares show comparable results to PSA samples for the same exposure time in good agreement with comparable states of the fractured surfaces shown in Fig. 5.

$$\tau_{max}|_{T_i} = \frac{1}{2\pi f_{max}}|_{T_i} \quad \text{(Eq. 3)}$$

where τ_{max} is the conductivity relaxation time and f_{max} is the frequency corresponding to M''_{max} at at given temperature T_i.

Fig. 4d shows the τ_{max} values at −50 °C as function of the exposure time to salt fog spray testing for the two studied adhesive bond systems (Figure D1 shows same plot for other temperatures). Both systems (TFSAA and PSA) show same relaxation times before exposure (as-produced, time 0 days). Nevertheless, the systems behave significantly different with the exposure time to NSS. A clear decrease in the relaxation time with the exposure time can be observed for the TFSAA panel series (M'' peaks shift towards higher frequencies, drop of τ_{max} at 45 days in Fig. 4d). This suggests faster ionic motion attributed to an increase in number density of charge carriers, ion charges and mobility of the ionic species with the exposure time likely due to more salt solution ingress. The PSA series on the other hand shows relatively stable relaxation times with the exposure time, which remain two to three orders of magnitude higher than those of TFSAA. This suggests a lower impact of the exposure to the NSS environment in the PSA series. Similar trends were obtained for the other studied temperatures (Figure D1).

As shown in Fig. 4d and Figure D1, PSA duplicates at 90 and 180 days showed a high level of reproducibility with slightly varying τ_{max} (the variation increases at 180 days exposure). The two samples of TFSAA at equal exposure times (90 and 180 days) show different BDS results: up to four orders of magnitude difference in τ_{max} (Fig. 4d and D.1). Interestingly, the two TFSAA specimens showing higher τ_{max} values comparable to those of the PSA specimens at comparably long exposure times (samples #7 and #6 highlighted in Fig. 4d with black squares) showed also a higher percentage of cohesive fracture mode and less corrosion than the TFSAA samples for the same exposure times with low τ_{max} values (Fig. 5). The correlation between the BDS parameter and the state of the fractured bond interface suggests BDS is sensitive to the degradation degree of the adhesively bonded structure as seen with all the specimens tested in this work.

3.3. Destructive testing: floating roller peel tests and BLC evaluation

The mechanical performance of the adhesive bonds before and after exposure to the NSS was evaluated by measuring the peel strengths of two sample series using dry-wet peel for the as-produced samples and dry peel for the samples exposed to NSS. Once the samples were peeled open and their fracture load progression recorded, the crack fracture planes (Fig. 5a and b, Table E1) were optically analyzed to obtain the cohesive-interfacial failure contribution and the so-called bondline corrosion (BLC) parameter with the exposure time (Fig. 5e).

As can be seen in the photos of the fractured specimens in Fig. 5a and b and Table E1 (including the samples studied by BDS), bondline corrosion is not homogeneous along the samples and the corrosion front progresses from the sides exposed to the salt fog spray environment into the specimen in different degrees [6]. The variations in the peel strength with the displacement (Table E1) show locations where such heterogeneities in the bond line take place. However, from these figures it is not possible to predict, where corrosion will start first.

Fig. 5b shows the average peel strength for both adhesive bond series as function of the exposure time. Although the adhesive bond strength of both series is similar prior to exposure to NSS, a significant decrease of bond strength with the exposure time can be seen for the TFSAA series. This indicates a lower durability of this anodizing process compared to that of PSA when the same adhesive bond protocol is used. Moreover, the peel load profiles of the PSA samples (Table E1) are more stable than those of the TFSAA, which indicates a more homogeneous bond stability

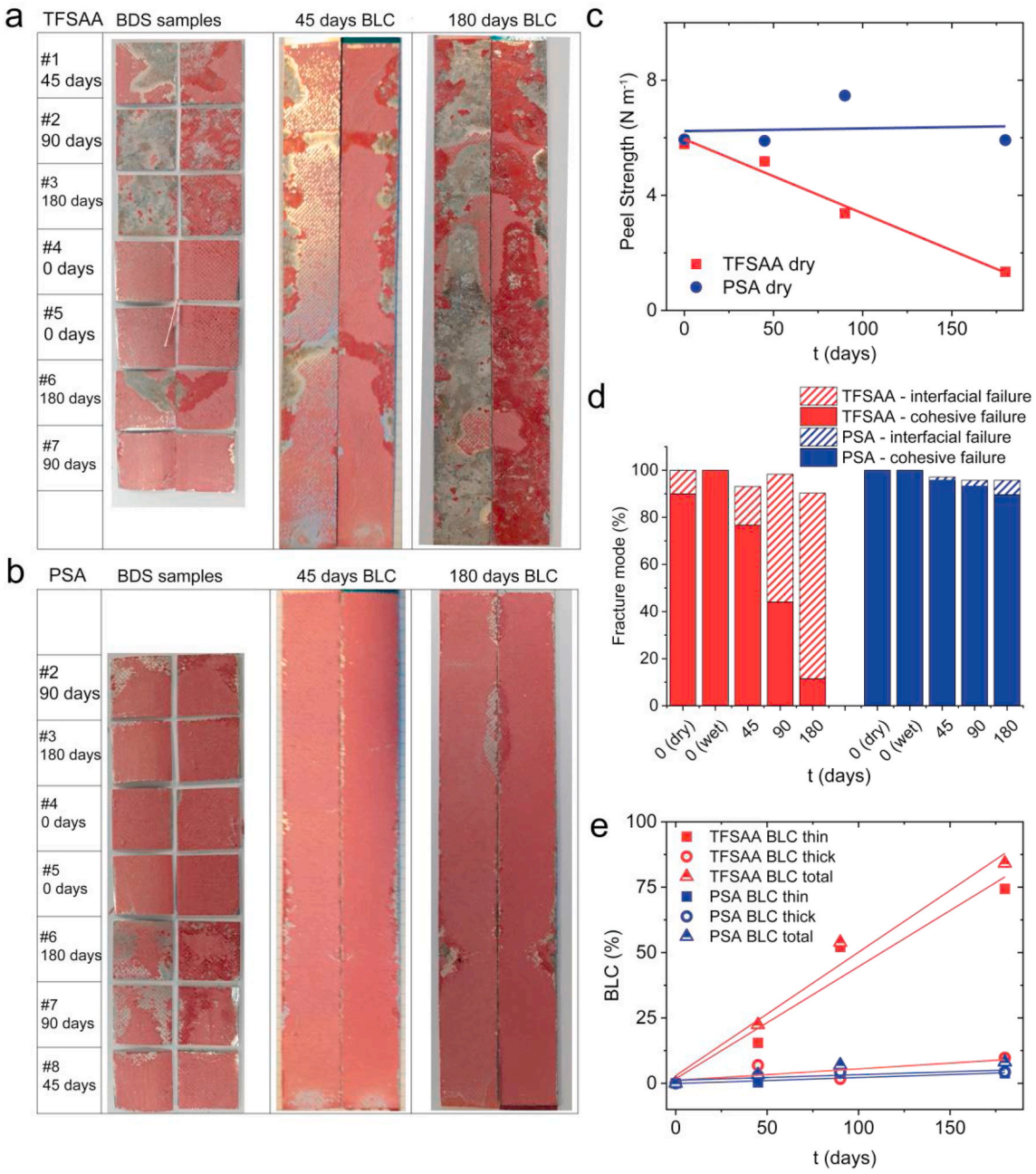

Fig. 5. Representation of opened BDS samples according to their position respect the FRP specimens for TFSAA (a) and PSA (b) where the BDS samples, the 45 days BLC specimen and 180 days BLC specimen are shown at the left, middle and right respectively. Individual images show thin adherend present on the thin (left) and thick (right) adherends of each sample. (c) Peel strength of the panels TFSAA and PSA after exposure times of 0, 45, 90 and 180 days. (d) Fracture modes of the panels, determined by visual analysis of the surfaces highlighting the distribution of the different failure modes. (e) BLC results for panels TFSAA and PSA as function of exposure time show more corrosion in the thin adherend panel of the TFSAA sample.

in the PSA case.

Visual inspection of the panels after the floating roller peel test (Table E1) allowed classifying the failure mode for each exposure time as function of the interfacial failure percentage (i.e. unwanted failure at the metal-adhesive interface and called as adhesive failure according to the manufacturing terminology) and cohesive failure (i.e. crack propagating through the adhesive). Fig. 5d shows the contribution of each failure modes to the whole peeled strip for each exposure time. Both as-produced samples (0 days) showed mainly cohesive failure in the wet-dry peel test. In this test the wet and dry events can be separated as the moment of water adhesion during the peel test is known. This leads to two columns in Fig. 5d (dry and wet) related to 0 days. Cohesive failure dominance was observed in all four cases with a small interfacial (adhesive) failure contribution in the case of dry-test of the TFSAA sample. The PSA series kept showing cohesive failure with the exposure to NSS while the TFSAA series showed a decrease of the cohesive failure with the exposure time, clear sign of interfacial degradation due to water and salt ingress.

The progression of the bondline corrosion with time is shown in Fig. 5e and is calculated as the area covered by oxides observed during optical inspection of the opened strips. In the case of the PSA series, both the thin and the thick adherends of the tested panels show comparably limited amount of corrosion and mostly cohesive fracture mode. For the TFSAA series, most of the corrosion is on the thin adherend. This effect could be related to a higher sensitivity of the TFSAA process to the thickness of the clad aluminium alloy layer, which is thinner for the

thinner sheet, leading to a less stable oxide-metal substrate interface in this anodizing process. The decrease of the peel strength can thereby be directly attributed to the progression of corrosion in this case.

3.4. Correlation between BDS and peel testing

From the previous section, it becomes apparent that BDS is as capable as peel testing to identify that the TFSAA system is less durable than PSA yet in an NDT manner.

Visual analysis of the samples (Fig. 5 a-b) confirmed inhomogeneity in the corrosion progression over the samples and a discrepancy between the BLC panels and the smaller specimens prepared for BDS analysis. In the same figure, the origin of the samples used in BDS with respect to the panels from where they were cut off and the samples used in peel testing can be seen, with no clear position-dependent result. The opening of the samples after the BDS testing was performed in a comparable way as for those from the floating roller peel test. Clear differences in fracture mode and corrosion degree between samples exposed for the same time to the NSS can be identified. For example, TFSAA_#7_90 days shows cohesive failure without corrosion while TFSAA_#2_90 days show extensive corrosion. This is in good agreement with the BDS results (Fig. 4d), where the sample TFSAA_#7_90 days showed similar τ_{max} to the PSA samples, both showing mostly cohesive failure. A similar observation can be made for the samples exposed for 180 days where TFSAA_#6_180 shows higher cohesive failure and lower corrosion than TFSAA_#3_180 I good agreement with a higher τ_{max} for the first. These results reflect on the ability of BDS to discriminate between an adhesive bond in good state after exposure to NSS and one showing clear a bond interfacial degradation.

In an attempt to make the BDS analysis protocol proposed here more quantitative in relation to the type and extent of the bond failure in order to use it as an NDT to analyze during-use bonds, the results from the BDS were compared with those obtained from the optical analysis and those from the mechanical peel test (Table F1). Fig. 6a and b shows the relation between the three classification parameters used so far to study the bond strength: (i) peel strength from mechanical testing, (ii) adhesion failure component (% of interfacial failure) from mechanical testing and from the samples used in BDS, and (iii) the apparent relaxation time, τ_{max}, obtained from BDS with the electric modulus formalism. In order to correct for the local heterogeneities, the apparent relaxation time was related to the failure mode from the BDS samples and not to the interfacial failure from the BLC samples (Fig. 6b). A clear relation between the percentage of interfacial failure and the peel strength (Fig. 6a) and between the percentage of interfacial failure and the apparent relaxation time (Fig. 6b) is visible. As it can be seen, BDS allows the grouping of the samples in three distinctive failure behaviors (cohesive, interfacial, and interfacial + corrosion) depending on their τ_{max} values. In this representation, the two TFSAA samples tested at 90 and 180 days exposure to NSS that gave results similar to those of the PSA treatment (#7 and #6) are included under cohesive and interfacial failure instead of interfacial + corrosion. High values of τ_{max} (higher than 10^{-2} s for the example shown obtained at −50 °C) correspond to good durability bonds with cohesive failure when cracked opened (Fig. 6b), which in turn correspond to samples giving aerospace 'acceptable' peel strength values (higher than 5.5 N/m according to AITM5-009) and very low interfacial failure component (% of interfacial failure) as shown in Fig. 6a. Although more dedicated studies about variability in data and quantification are necessary, the results highlight the high sensitivity of the BDS method to the state of interfacial adhesion. The electric modulus formalism is capable to determine the quality of the bond and the expected interfacial degradation degree, and shows its potential for use in research of interactions and degradation behaviour of the anodic oxide –

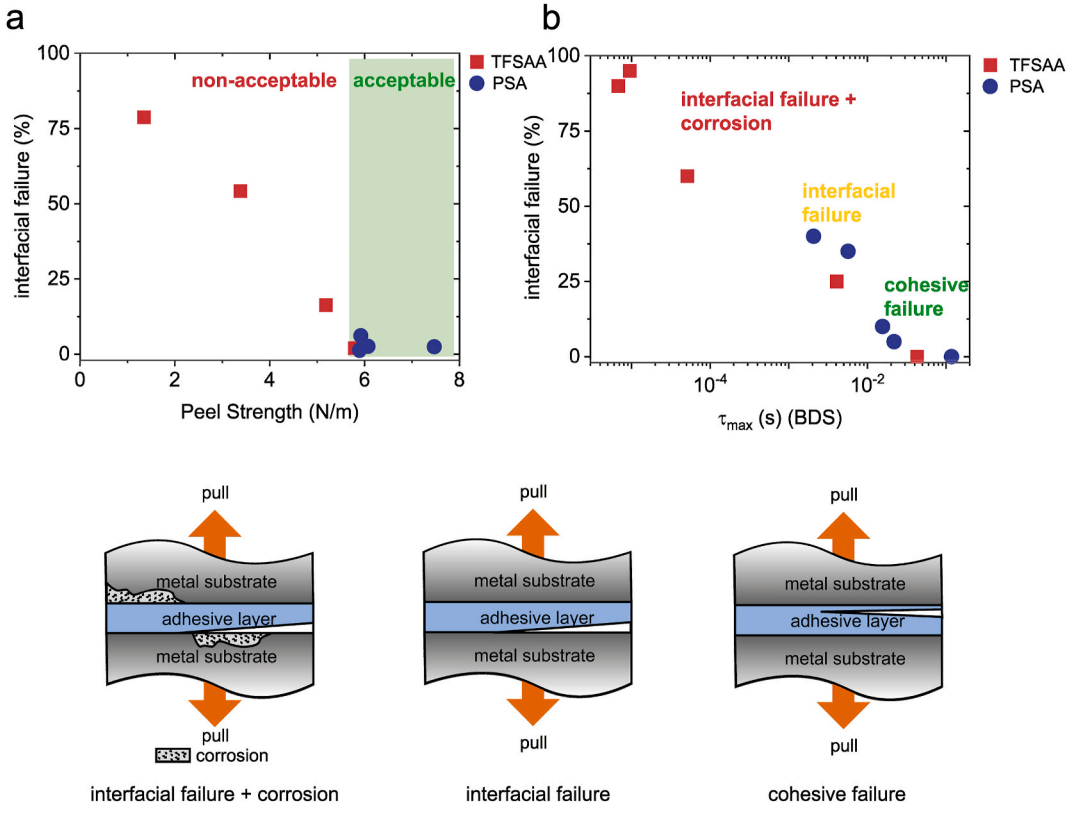

Fig. 6. (a) Relation of the peel strength (mechanical tests results) and the apparent conductivity relaxation time (τ_{max}) obtained with BDS at −50 °C (b) with the failure mode measured by post-mortem optics analysis of the BLC samples and between and the post-mortem optics analysis (interfacial failure percentage) of the samples tested in the BDS). Acceptable and non-acceptable bond strength limits in Fig. 6a are established based on AITM5-009. Figures show the high potential of BDS to determine the state of the bond through the use of τ_{max} from the electric modulus formalism.

adhesive systems.

4. Conclusions

Broadband dielectric spectroscopy (BDS) and mechanical testing were used to test the durability and bond strength of adhesive bonds using two anodizing protocols. Both destructive and non-destructive tests correlate well and confirm that the PSA process, producing "bird-nest" structures, larger pores and layer thickness, results in durable adhesion and low bondline corrosion. Broadband dielectric spectroscopy was able to monitor the interfacial degradation state with the exposure time to NSS and hence reveal the state of the adhesive bond in a nondestructive manner.

The apparent conductivity relaxation time (τ_{max}) obtained from the use of the electric modulus formalism is proposed as a predictive BDS parameter to differentiate between as-produced high and low quality bonds. Moreover, the same parameter was able to differentiate the state of the bond upon exposure to NSS distinguishing between three performance modes as function of the τ_{max} value: cohesive failure, interfacial (adhesive) failure, and interfacial failure with corrosion. The samples identified with cohesive failure by BDS show very good agreement with the peel strength values obtained through destructive mechanical evaluation by FRP/BLC testing, which in turn correspond to commonly defined as 'acceptable' adhesive bonds.

The sensitivity of the BDS protocol allowed to identify the presence of mixed modes of interfacial failure. Unlike traditional destructive testing methods, where inhomogeneity in corrosion progression is to a lesser extent taken into account, this work provides the first proof-of-concept indication that BDS can be used to identify local interfacial failure and corrosion in a non-destructive manner. The capability of detecting the first stages of adhesive bond degradation and the transition to interfacial weakening and subsequent corrosion opens the door to further studies on degradation protocols, processing parameters, anodizing processes and adhesive chemistries and their effect on the durability of adhesive bonds using NDT.

All data supporting the findings of this study are available within the article and in the Supplementary Information.

Acknowledgements

The authors acknowledge the financial support from TU Delft and GKN Fokker Aerostructures. The authors acknowledge B. Poker for executing the pre-treatments, M. Lambermont and L. van Tiggelen for adhesive bonding and mechanical testing. The authors thank F. Oostrum for his advice on SEM.

Appendix A. Supplementary data

Supplementary data to this article can be found online at https://doi.org/10.1016/j.ijadhadh.2022.103246.

References

[1] Jeevi G, Nayak SK, Abdul Kader M. Review on adhesive joints and their application in hybrid composite structures. J Adhes Sci Technol 2019;33:1497–520.
[2] Budhe S, Banea MD, de Barros S, da Silva LFM. An updated review of adhesively bonded joints in composite materials. Int J Adhesion Adhes 2017;72:30–42.
[3] Abrahami ST, Hauffman T, de Kok JMM, Mol JMC, Terryn H. XPS analysis of the surface chemistry and interfacial bonding of barrier-type Cr(VI)-Free anodic oxides. J Phys Chem C 2015;119:19967–75.
[4] Abrahami ST, de Kok JMM, Gudla VC, Ambat R, Terryn H, Mol JMC. Interface strength and degradation of adhesively bonded porous aluminum oxides. Mater. Degradation. 2017;1:8.
[5] Viana G, Costa M, Banea MD, da Silva LFM. A review on the temperature and moisture degradation of adhesive joints. Proc IME J Mater Des Appl 2016;231:488–501.
[6] Determination of resistance to bond line corrosion., in: AITM 5-0009, Airbus, [Nordenham].
[7] Standard practice for operating salt spray (fog) apparatus. In: Astm B117-16. West Conshohoken, PA: ASTM International; 2018.
[8] Pethrick RA. Design and ageing of adhesives for structural adhesive bonding – a review. Proc IME J Mater Des Appl 2014;229:349–79.
[9] Maeva E, Severina I, Bondarenko S, Chapman G, O'Neill B, Severin F, Maev RG. Acoustical methods for the investigation of adhesively bonded structures: a review. Can J Phys 2004;82:981–1025.
[10] Tattersall HG. The ultrasonic pulse-echo technique as applied to adhesion testing. J Phys Appl Phys 1973;6:819–32.
[11] Her S-C, Lin Y-C. Assessment of adhesive bond strength using the ultrasonic technique. J Adhes 2014;90:545–54.
[12] Ciampa F, Mahmoodi P, Pinto F, Meo M. Recent advances in active infrared thermography for non-destructive testing of aerospace components. Sensors 2018;18:609.
[13] Silva LFMd, Öchsner A, Adams RD. Handbook of adhesion technology. Cham: Springer; 2018.
[14] Bossi R, Housen K, Walters C. Laser bond inspection device for composites: has the holy grail been found? NTIAC Newsletter 2005;30.
[15] Kaufman J, Böhm M, Brajer J, Zulic S. Laser shock peening of aluminium alloys to enhance surface properties. MM Sci. J. 2019:3638–42.
[16] Kremer F, Schonhals A. Broadband dielectric spectroscopy. Springer; 2003.
[17] Rathi A, Hernández M, Garcia SJ, Dierkes WK, Noordermeer JWM, Bergmann C, Trimbach J, Blume A. Identifying the effect of aromatic oil on the individual component dynamics of S-SBR/BR blends by broadband dielectric spectroscopy. J Polym Sci B Polym Phys 2018;56:842–54.
[18] Maity P, Poovamma PK, Basu S, Parameswaran V, Gupta N. Dielectric spectroscopy of epoxy resin with and without nanometric alumina fillers. IEEE Trans Dielectr Electr Insul 2009;16:1481–8.
[19] Li Y, Krentz TM, Wang L, Benicewicz BC, Schadler LS. Ligand engineering of polymer nanocomposites: from the simple to the complex. ACS Appl Mater Interfaces 2014;6:6005–21.
[20] Hernández M, Grande AM, van der Zwaag S, García SJ. Monitoring network and interfacial healing processes by broadband dielectric spectroscopy: a case study on natural rubber. ACS Appl Mater Interfaces 2016;8:10647–56.
[21] Wübbenhorst M, Napolitano S. Deviations from bulk glass transition dynamics of small molecule glass formers: some scenarios in relation to the dimensionality of the confining geometry. In: Kremer F, editor. Dynamics in geometrical confinement. Cham: Springer International Publishing; 2014. p. 247–77.
[22] Banerjee PK, Elenchezhian MRP, Shute N, Vadlamudi V, Raihan R, Reifsnider K. Predicting adhesive bond performance based on initial dielectric properties. In: Proceedings of the American society for composites—thirty-second technical conference 2017; 2017.
[23] Elenchezhian MRP, Vadlamudi V, Banerjee P, Dave C, Mahmood A, Raihan R, Reifsnider K. Quality assessment of adhesive bond based on dielectric properties. In: Society of the advancement of material and process engineering. SAMPE); 2017.
[24] Tsangaris GM, Psarras GC, Kouloumbi N. Electric modulus and interfacial polarization in composite polymeric systems. J Mater Sci 1998;33:2027–37.
[25] McCrum NG, Read BE, Williams G. Anelastic and dielectric effects in polymeric solids. New York: Wiley; 1967. p. 617. Journal of Applied Polymer Science, 13 (1969) 397-397.
[26] De Kok JMM, Van den Heuvel VKJ. In: Method of anodizing an article of aluminium or alloy thereof; 2016, WO2017183965A1.
[27] AIPS02-01-006. Airbus process specification phosphoric sulphuric anodising (PSA) of aluminium alloys prior to structural bonding.
[28] Hart-Smith LJ. A peel-type durability test coupon to assess interfaces in bonded, co-bonded, and co-cured composite structures. Int J Adhesion Adhes 1999;19:181–91.
[29] Britton RA. In: Acceptance criteria for aerospace structural adhesives. Defense Technical Information Center; 1978.
[30] Hart-Smith LJ. Reliable nondestructive inspection of adhesively bonded metallic structures without any instruments. In: Materials challenge: diversification and the future. Covina CA: Society for the Advancement of Material and Process Engineering (SAMPE); 1995. 40 - Book II.
[31] DIN 65448 Aerospace; structural adhesives; wedge test.; 1988. p. 8.
[32] Peterson EE, Arnold DB. Relationship of interfacial compatibility to durability of adhesive - bonded joints. In: Air force wright aeronautical laboratories technical report, AFWAL-TR-80-4176; 1981.
[33] Hassan MK, Tucker SJ, Abukmail A, Wiggins JS, Mauritz KA. Polymer chain dynamics in epoxy based composites as investigated by broadband dielectric spectroscopy. Arab J Chem 2016;9:305–15.
[34] Johari GP. Intrinsic mobility of molecular glasses. J Chem Phys 1973;58:1766–70.
[35] 3M. In: 3M scotch-weld structural adhesive film AF 163-2 technical datasheet; 2009.
[36] Roling B. What do electrical conductivity and electrical modulus spectra tell us about the mechanisms of ion transport processes in melts, glasses, and crystals? J Non-Cryst Solids 1999;244:34–43.
[37] Richert R. The modulus of dielectric and conductive materials and its modification by high electric fields. J Non-Cryst Solids 2002;305:29–39.
[38] Migahed MD, Ishra M, Fahmy T, Barakat A. Electric modulus and AC conductivity studies in conducting PPy composite films at low temperature. J Phys Chem Solid 2004;65:1121–5.
[39] Hodge IM, Ngai KL, Moynihan CT. Comments on the electric modulus function. J Non-Cryst Solids 2005;351:104–15.